International Forum on Aeroelasticity and Structural Dynamics
IFASD 2017
25-28 June 2017, Como - Italy

DEVELOPMENT OF A BUFFET LOAD MITIGATION SYSTEM BASED ON MULTI-SURFACE CONTROL

Sheharyar Malik[1], Luca Riccobene[1], Sergio Ricci[1] and Daniele Monti[2]

[1] Dipartimento di Scienze e Tecnologie Aerospaziali
Politecnico di Milano
sheharyar.malik@polimi.it

[1] Dipartimento di Scienze e Tecnologie Aerospaziali
Politecnico di Milano
luca.riccobene@polimi.it

[1] Dipartimento di Scienze e Tecnologie Aerospaziali
Politecnico di Milano
sergio.ricci@polimi.it

[2] LEONARDO Company, Aircraft Division,
Venegono Superiore, VA, ITALY
daniele.monti@leonardocompany.com

Keywords: Mitigation, Aeroelasticity, Uncertainty, Buffet, Airbrake, and Hankel.

Abstract: This paper presents the numerical and experimental research activity aiming at the implementation of a Buffet Load Mitigation System (BLMS). Motivated by the advantages associated with the multi surface control, movable leading and trailing edges are actively controlled through static output feedback suboptimal controller. Scaled wing model of X-DIA was analyzed numerically for structural, aerodynamic and aeroelastic analysis by using MSC/NASTRAN. State space realization was completed by in-house built aeroelastic software MASSA founded on MATLAB. Deterministic and probabilistic optimization algorithms optimized the suboptimal controller. Levenberg-Marquardt algorithm founded on second order quadratic formulation ousted further candidates for its robustness and efficiency. Hankel singular values (HSV) validated the sensor/actuator configuration on the wing, precedingly configured on the principle of Identical location of Actuator and Sensor (ILAF) law. HSV defined the unified theme in comparative study of the wing. Application of notch filters on the output feedback and uncertainties were incorporated in the model by built-in MATLAB functions. Robustness of the BLMS under uncertainties was experimentally realized by changing sensitivity of accelerometers and incorporating efficiency factor with the output of PID_2. Numerical analyses predicted good performance for wind tunnel experiments. Airbrake installed upstream of the wing replicated the buffet loads in the wind tunnel test section. Considerable attenuation was demonstrated for wing first bending and torsion modes by the active control systems. Power spectral estimates and densities and frequency response are presented to highlight the achieved results.

1 INTRODUCTION

New aircrafts can deliver high performance under different flight conditions. This advantage poses many restrictions on structural capability and aerodynamic performance of the aircraft. Thus, a tradeoff is needed between high performance and structure, aerodynamic capability, or aircraft should be equipped with new advanced systems to withstand loads at high performance [1]. In the case of high performance aircraft, such as advanced trainers, aiming at enhanced performances at high angle of attack, unsteady, turbulent flow is formed from the nacelle, nose and canard of the aircraft, which results in variable pressure across the aircraft, causing fluctuating stresses on the wings and vertical tail of the aircraft. This phenomenon is commonly called buffeting and it is usually apparent at high angle of attack. Two types of buffeting phenomena are usually reported: buffet onset due to the flow separation at high turn rates that is primarily responsible for stresses on the outboard wing. A second source of buffeting loads is due to vortical flow that is generated from the nose of the aircraft and is responsible for stresses on inboard wing and vertical tail of the aircraft. [2]. Apart from imparting stability to the aircraft, the advancement in the control techniques has allowed the increased contribution of control surfaces to suppress vibrations and load control. Sensocraft and blended wing body are just a couple of examples of it [3, 4]: by employing advanced control strategies, the static and dynamic aeroelastic loads can be redistributed on the wing to mitigates the structural deformation and delay the flutter occurrences respectively [5, 6]. Suboptimal controller based on quadratic formulation is used to attenuate the gust loads by using active ailerons in [7]. Significance of attenuating dynamic loads by multiple control surfaces located on the leading and trailing edges of the wing is highlighted in [8].

As a general remark, the usage of multiple control surfaces ensures more degrees of freedom in the design of adaptive and robust wing. In case of multiple possibilities, Hankel singular values (HSV) shows the promise to optimize the control strategy and cost function by utilizing the suitable combinations of actuators and sensors [9]. Application of notch filters on output feedback without affecting the system dynamics for participating frequencies has been devised by [10, 11]. Output feedback of the system has been used by [12], to check the adaptiveness and robustness of the system. Parametric uncertainties in the actuator model is introduced to check the robustness of the formulated controller [13, 14]. While both passive and active techniques are used to delay, or to alleviate the buffeting phenomena, in this research the focus is directed towards the active implementation of control techniques to reduce buffeting loads. The work presented here includes the description of the approach, the implementation on the already available wind tunnel model, X-DIA, and finally the results of the experimental campaign allowing to validate the proposed approach.

The aeroelastic demonstrator X-DIA, shown in Figure 1, was built at Politecnico di Milano under the European research project 3AS [15 16]. It is a 1/10 constant Froude scaled model of an advanced configuration regional aircraft. X-DIA is an unconventional aircraft with T-tail, forward swept (-15 deg), wing dihedral of (+3 deg) with all moveable canard. The reference full scale aircraft can carry up to 80 passengers with cruise speed of 400 kt and ceiling of 26,250 ft. T-tail and the main wing are attached at the end of the fuselage. The aircraft wing is constructed as to ensure distributed flexibility to replicate the true aeroelastic model associated phenomenon. Each half wing of the X-DIA is equipped with four control surfaces; two are located at the leading edge (inboard and outboard) and two are located on the trailing edge (inboard and outboard). These surfaces are named as LEI, LEO and TEI, TEO respectively. The schematic of the wing is shown in figure 2.

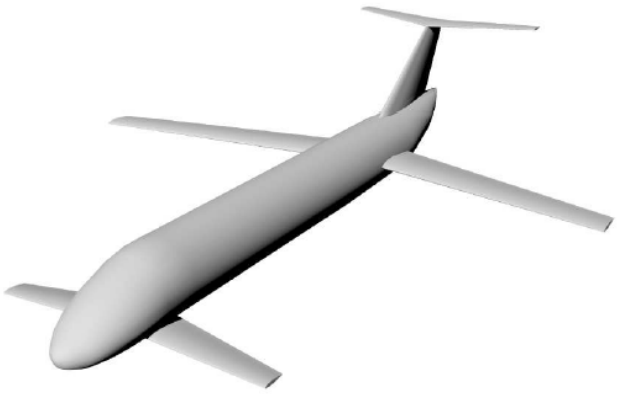

Figure 1: X□DIA CAD Model

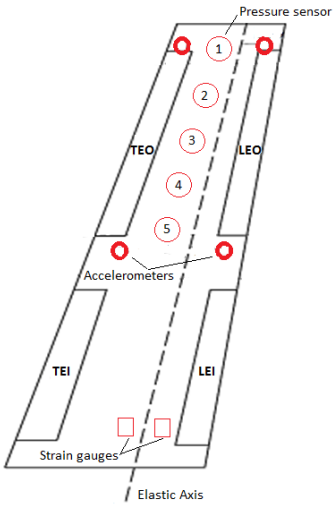

Figure 2: X-DIA wing

The control strategy adopted previously was built on the well know ILAF approach [17]. Four accelerometers were placed in each wing, two on the wing tip and two at mid span of the wing. The actuators were chosen by keeping in view the static and dynamic performance criteria for this analysis i.e. bandwidth, phase lag and continuous torque. The bandwidth of the electric actuators driving the control surfaces is about 30 Hz, which satisfies the desired operational range [17]. Starting from already available analytical model, numerical analyses were performed to predict the wing behavior. The control scheme defined in the proceeding sections was designed and validated during an experimental campaign at Politecnico di Milano-Department of Aerospace Science and Technology in the De Ponte wind tunnel. Airbrake was manufactured to simulate the buffet loads in the test section. Upper surface of the wing was equipped with piezo resistive pressure transducers to analyses the power spectrum of buffeting loads. X-DIA wing specifications are shown in table 1. In the upcoming sections, complete detail is presented for numerical modelling, optimization strategy, experimental setup and collected results.

X-DIA right wing specification		
Wing span	1.5	m
Wing surface	0.75	m^2
Wing sweep	15	deg
Wing dihedral	3	deg
Total Mass	2.4	Kg

Table 1: X-DIA right wing specifications

2 AEROSERVOELASTIC FORMULATION

Finite Element model of X-DIA wing has already been realized analytically [15], in the current activity numerical analysis formed the basis of structural model. MSC/NASTRAN provided the platform along with PATRAN to identify the normal modes and aeroelastic modes. Doublet Lattice Method (DLM), included in MSC/NASTRAN provided the aerodynamic model which admits the turbulent flow with high fidelity. Both structural and aerodynamic models were coupled by the in-house developed software MASSA, to form the aeroelastic state space model which lead out the basis of control systems. Complete time domain aeroelastic model can be furnished by selecting appropriate structural inputs for feedback along with aerodynamic outputs. The procedure is briefly explained here, for more

thorough study the reader is referred to [18]. As reported by [19], numerous strategies are available to model the unsteady aerodynamics, however rational matrix fraction approximation stands out in accuracy and forms the basis of aerodynamic model in this developed code. The unsteady aerodynamic response matrix can be derived by assuming minimal role of gust response matrix in the following equation:

$$f = H_{am}(k, M_\infty).q + H_{ag}(k, M_\infty).\frac{V_g}{V_\infty} \tag{13}$$

Aerodynamic forces can be approximated by Rogers technique [20]:

$$H_{am} = D_o + D_1 p + D_2 p^2 + \sum_{i=1}^{m} \frac{p}{p + \beta_i} E_i \tag{14}$$

'β' is the user defined poles with real part to be negative to assure stability. In literature approximations based on Pade's principal can also be found [21]. The aeroelastic state space model of the complete system takes the form:

$$\dot{x} = Ax + Bu \qquad y = Cx + Du \tag{15}$$

While solving the following aeroelastic model equations:

$$E_{ae}\dot{x}_{ae} = A_{ae}x_{ae} + B_{ae}f$$

Where

$$E_{ae} = \begin{bmatrix} M_{ae} & 0 & 0 \\ 0 & I & 0 \\ 0 & 0 & I \end{bmatrix} \quad \dot{x}_{ae} = \begin{Bmatrix} \{\delta_i\} \\ q \\ \{\delta_{ir}\} \\ r \\ x_{ae} \end{Bmatrix} \tag{16}$$

where 'q' and 'r' represents the generalized degree of freedom and virtual states respectively. Actuator dynamics is incorporated to complete the aeroservoelastic model, the behavior of control surface under hinge moments can be given as:

$$\{\delta_i\} = [H_\delta]\{\delta_{c,i}\} \tag{17}$$

The complete aeroservoelastic model served as the basis of buffet load mitigation system. It consists of total 108 aeroelastic states. Summary of the extracted results is shown in table 2:

Mode no.	Frequency, Hz	Mode shape
1	9.390	1st bending mode
2	11.13	1st in plane bending mode
3	24.63	1st torsion mode
4	39.84	1st TEO bending mode
5	47.06	2nd bending mode

Table 2: Modal properties

3 CONTROL LAW FORMULATION

The flow dependent feedback can destabilize the wing through turbulent loadings. Aeroelastic phenomena can be grasped with high fidelity linear time invariant (LTI) state space models, low and higher order models can be built with compromise on fidelity level to predict the modes accurately [9]. The linear dynamics of aeroelastic model provides the eigenvector or singular analysis for stability analysis. The aeroservoelastic model realized from dynamic and aeroelastic numerical analysis in MSC/NASTRAN is formulated as state space based linear time invariant system:

$$\begin{aligned} \dot{x} &= Ax + B_u u + B_d d \\ y &= C_y x + D_{yu} u + D_{yd} d + n \\ z &= C_z x + D_{zu} u + D_{zd} d \end{aligned} \tag{6}$$

Where $x \in \square^n$ represents state vector, $u \in \square^{m_u}$ represents controlled input, $d \in \square^{m_d}$ represents turbulent input with appropriate shape filtering, $z \in R^l_z$ represents performance index. Feedback on the output u = -Gy, forms the vectorized gain matrix $G^{'} = (I + GD_{yu})^{-1}G$, the closed loop system with these assumptions is given as:

$$\begin{aligned} \dot{x} &= (A - B_u G C_y)x + [(B_d - B_u G D_{yd})d - (B_u G)n] = \bar{A}x + \bar{B}d \\ z &= (C_z - D_{zu} G C_y)x + [(D_{zd} - D_{zu} G D_{yd})d - (D_{zu} G)n] = \bar{C}x + \bar{D}d \end{aligned} \tag{7}$$

User defined objective function based on performance index and inputs is specified by:

$$F = E(z^{'} W_{zz} z + u^{'} W_{uu} u) \tag{8}$$

where ‘E’ depends on the external disturbances shaped by the white noise, with expansion of weighting functions, performance index and inputs, it is possible to express as the trace of covariance and solution of the Lyapunov equation for Controllability, above statement can be formulated as:

$$F = Tr(W_L P) \tag{9}$$

It finds the solutions by simultaneously solving the two Lyapunov equations, given by the following form:

$$\begin{aligned} \bar{A}P + P\bar{A}' &= -W_P \\ L\bar{A} + \bar{A}'L &= -W_L \end{aligned} \tag{10}$$

where $\mathbf{W}_L$ and $\mathbf{W}_P$ are defined for this specific case as:

$$\begin{aligned} W_P &= B_d^{'} W_d B_d - B_d^{'} W_d B_u G D_{yd} - D_{yd}^{'} G^{'} B_u^{'} W_d B_d + D_{yd}^{'} G^{'} B_u^{'} W_d B_u G D_{yd} \\ W_L &= C_z^{'} W_z C_z - C_z^{'} W_z D_{zu} G C_y - C_z D_{zu}^{'} G' C_y^{'} W_z + D_{zu}^{'} G^{'} C_y^{'} W_z D_{zu} G C_y \end{aligned} \tag{11}$$

It provides the basis of numerical optimization in this framework which can be constrained or unconstrained defined by the user. Second order quadratic formulation presented in [7], was analytically driven to exploit it in optimization procedures for the static output feedback controller. Exploiting singular values of controllability and observability gramian gives the relative conditioning of controllability and observability of the system. Gradient and hessian were formulated with respect to design variables, are presented in the impending section.

3.1 Optimization strategy

Common objective to all the optimization technique is the selection of effective cost function. BLMS was developed as such to exploit the different combinations of actuators and sensors for the beneficial attenuation of modes. HSV is used to measure the effective coupling of different parameters to maximize the design goals [22]. The conclusion is the selection of appropriate control surfaces along with sensors that will increase the control system efficiency and performance. The dynamics of the wing can be represented symbolically by the following transfer matrix in equation 12:

$$\begin{bmatrix} z \\ y \end{bmatrix} = \begin{bmatrix} P_{zw} & P_{zu} \\ P_{yw} & P_{yu} \end{bmatrix} \begin{bmatrix} w \\ u \end{bmatrix} \tag{12}$$

The transfer matrix P_{zw}, is the path to performance from input disturbance signals and the transfer matrix $P_{yu,}$ define the path from the input actuator or signal to the response of the sensor. The performance criteria and feedback of the system are analogous. Identical location of accelerations and forces is also validated by this control scheme. The present optimization strategy can switch between different input-output signals for already mentioned transfer matrices, gives the advantage to readily enhance the performance and robustness of the system.

The control scheme includes weighting functions for the trade of between control effort and performance successfully, as implemented in LQG problem for typical section airfoil [23]. With few changes in control the wing can be divided into inner and outer strip, leading edge and trailing edge strip or a single control surface working independently to attenuate the unwanted loads. The control scheme is given in the figure 3:

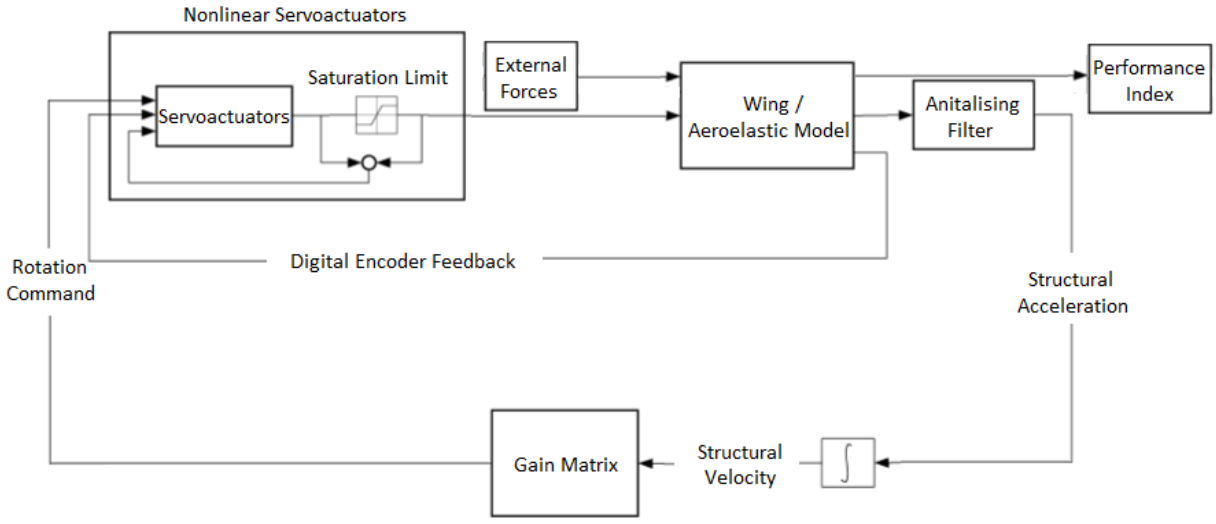

Figure 3: Control schematic of BLMS

4 OPTIMIZATION ALGORITHM

Heuristic optimization techniques were devotedly analyzed for static output feedback control. Algorithms based on deterministic and stochastic schematic were formulated, implemented and inferences were made based on convergence rate and robustness criteria. Deterministic Algorithms include first order and second order systems.

1. Gradient Descent Method (Analytical).
2. Gradient Descent Method (Numerical).
3. Newton's Method.
4. Levenberg-Marquardt Method.
5. Genetic Algorithm.

Gradient descent method established the basis for of optimization. Another method reported in literature 'Levenberg Marquardt' combines the beneficial features of gradient descent and newton's method. It behaves like newton's method in vicinity of the solution and subsequently as gradient descent when away from the solution and accelerates towards the solution. It does so by exploiting the advantages associated to variable step length. Given the objective function $F(g) \in \square^n$, gradient $J(g) \in \square^n$ was computed by analytically formulating the method presented for second order quadratic formulation in [7]. The hessian $H(g) \in \square^{n \times n}$ can be computed in the following form:

$$H = J^T J + \lambda^2 (J^T J) \tag{1}$$

Iterative procedure given by $g^{k+1} = g^k - H^{-1} \times \nabla J$, reduces the given objective function. Solution to gradient descent methods can found by solving the first order iterative procedure $g^{k+1} = g^k - \alpha \nabla J$, α represents the step length. Initial step length was calculated as mentioned in [24]. The idea of variable step size was implemented for gradient descent by establishing a relationship to update the gradient at the next step in the following form:

$$\alpha_K = \nabla f_k^T p_k / p_K^T Q p_k \tag{2}$$

α_k represents the step size in current iteration. Efficiency of the optimization can be increased by quasi newton method updates. First and second order systems are computationally expensive, which can be avoided by using derivative free stochastic algorithms based on genetic evolution with reportedly better ratio of minimizing the cost function globally. Vector evaluated genetic algorithm proposed by J. D. Schaffer [25] was used. It selects non-dominated solutions and uses ranks to define the fitness. Old populations with less probability of survival is replaced by new off springs. Number of elements 'k' in starting population gives clue about string length, $2^l \geq k$, Probability for crossover and mutation is between 0.6--1.0 and (1/population size – 1/string length) respectively. Penalty function guided the solution to convergence criteria, conversely it also added computational deficiency.

Once the cost function is formulated the algorithms mentioned before will optimize the cost function in the feasible region, the first order theorem will find the convergence by evaluating the gradients defined by the form [7]:

$$F_u = \mathrm{Tr}(W_{Lu} P + P_u W_L) \tag{3}$$

$$F_u = \mathrm{Tr}(W_{Lu}P + 2LA_uP + LW_{Pu}) \tag{4}$$

and the LM will minimize the cost functions by evaluating quadratic approximations of the form:

$$F_{uv} = \frac{1}{2}\mathrm{Tr}[W_{Luv}P + LW_{Puv} + 2L\bar{A}_{uv}P + (W_{Lu} + L\bar{A}_u + \bar{A}'_u L)P_v + (W_{Lv} + L\bar{A}_v + \bar{A}'_v L)P_u] \tag{5}$$

The optimization procedure is defined for stable system, so the system should be in asymptotically stable state for commencement of optimization algorithms. Constraints of the form maximum torque limit and power consumption of motor are dealt by the weighting functions introduced in the control system design. The robustness of the optimization algorithms was also tested for parametric uncertainties introduced in the numerical procedure for the nontrivial problems. Levenberg-Marquardt was set as the benchmark algorithm for optimization. It has been validated as suggested by the previous findings [26], that the convergence rate of Levenberg-Marquardt algorithms is faster than available optimization codes. Table 3, shows the comparison for different optimization algorithms.

Algorithm	Time(sec)
Gradient – Numerical	3.724
Gradient - Explicit	7.533
Newton's Method	3.639
Genetic Algorithm	9.097
Levenberg-Marquardt	3.400

Table 3: Efficiency of optimization algorithms

Figure 4, shows the optimization results for the candidate algorithms.

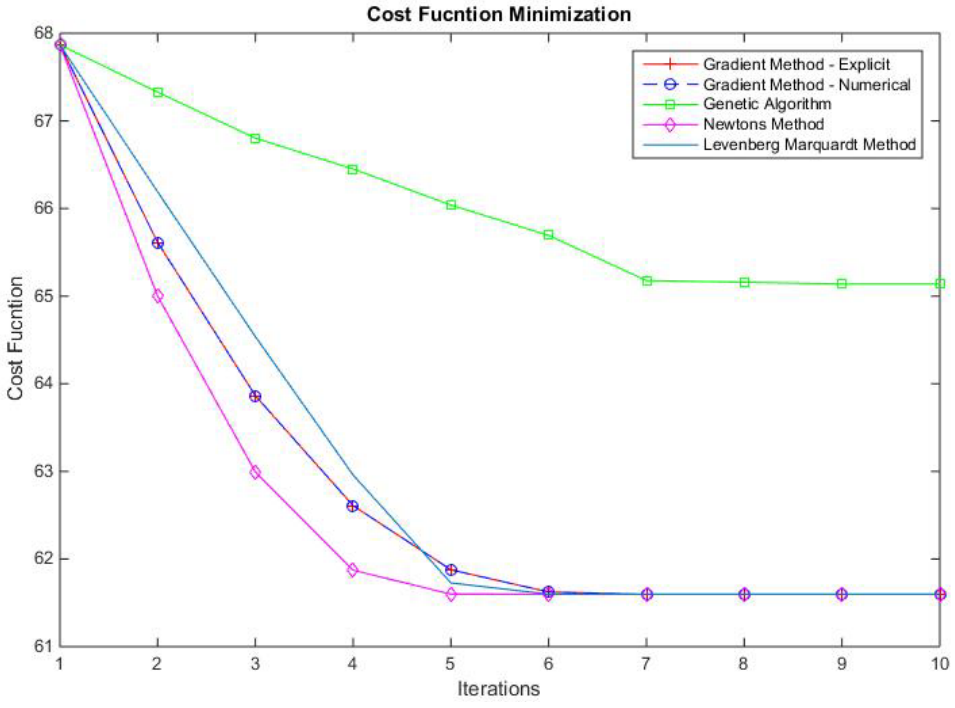

Figure 4: Cost function minimization

The results for Gradient-explicit and Gradient-numerical showed the high-fidelity approximation with the gradients provided numerically by the method presented in [7], Gradient-numerical method is almost twice efficient computationally. Numerical Frequency response evaluated by the abovementioned control law formulation and optimization strategy is shown figure 5. Active control system is shown for few cases; it is evident that BLMS significantly attenuates and damp the vibrations in the bending and torsion mode.

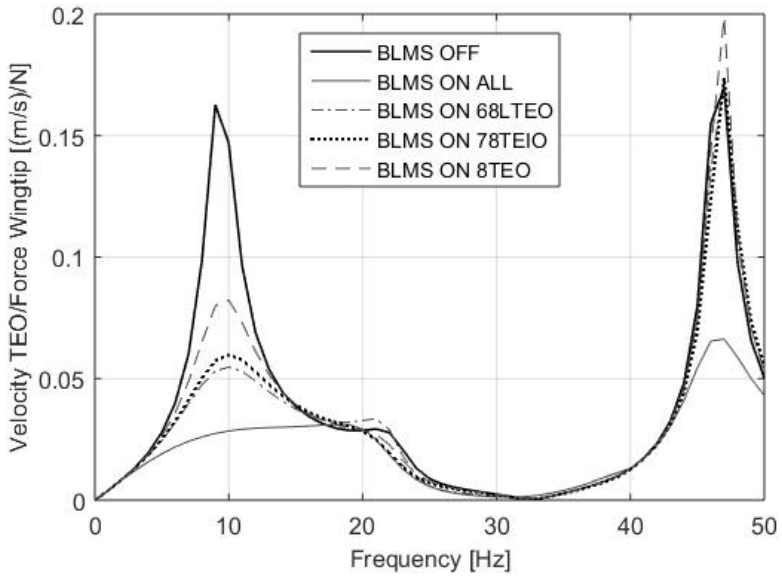

Figure 5: Numerical frequency response of BLMS

5 WINDTUNNEL TEST CAMPAIGN

The experimentation of buffet load mitigation system took place in March 2017 at Politecnico di Milano-Department of Aerospace Science and Technology, in the close circuit wind tunnel that has a rectangular cross section of 1.5×1 m^2. The wing was fixed at the center of the test section in vertical position by the help of custom made, load cells based balance system. Out-of-plane structural modes of the wing were identified by hammer roving method using LMS-TestLab software. Two test sections speeds (20m/s and 30 m/s) were selected for the experimental phase.

5.1 Airbrake system:

The airbrake was placed one meter ahead of the wing in the horizontal direction. The angle of the airbrake was varied from 20^o to 40^o degree, to produce the transverse and longitudinal vortices, that demonstrates the ability to excite the bending and torsion modes. The angle of attack of wing was fixed at 6.5^o. Figure 6, shows the airbrake and wing setup in the wind tunnel.

Figure 6: Airbrake system

Power spectral estimate is shown in the figure 7, for the excited frequencies by the airbrake at 30m/s (Positions can be noted from Instrumentation diagram of the wing, figure 2).

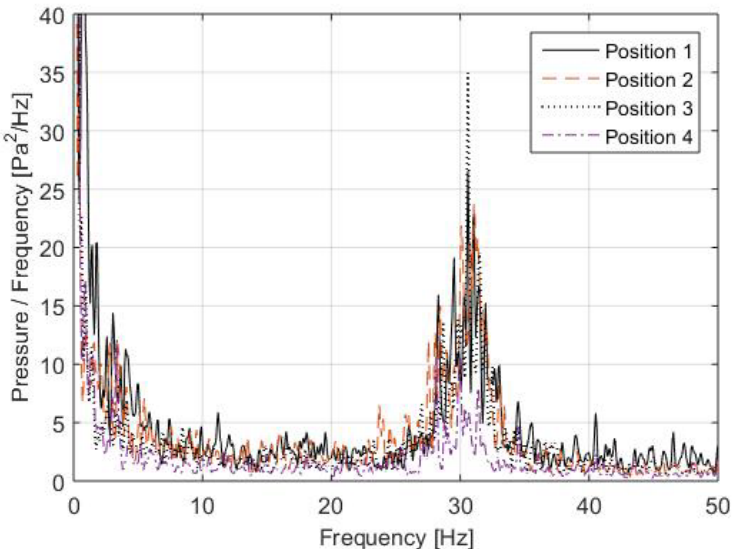

Figure 7: Power spectral estimate of pressure fluctuation at different positions

5.2 Instrumentation

PCB ICP Monoaxial Piezoelectric transducers (accelerometers) with sensitivity of 100mV/g were used to measure out-of-plane accelerations, these accelerometers were placed at midspan and wing tip on leading and trailing edge (see figure 2). The accelerometers are conditioned

by a dedicated unit and then filtered by a low pass 6th order elliptical filter. The data acquisition is done by NI 6036 and NI 6713 boards, used as input and output boards respectively with drivers available readily at open source Comedi. The motors for driving four actuators were selected by fulfilling the physical design constraints such as weight and maximum allowable size by the authors [17]. Comparative study of static and dynamic characteristics showed the ideal motors for the X-DIA wing were Portescap mod 17N78-210E. Thanks to planetary gears in shaft/line torque transmission, main concern of torque and gear reduction were met by installing them on motor shaft. Leading edges actuators were equipped with gear ratio of 88, while the trailing edges were given the gear ratio of 22. Actuator motors were provided with encoders attached at the gear head, as expected and experienced, the minimum counter resolution provided by the encoder for leading and trailing edges was 0.06 deg and 0.23 deg respectively. Actuators capacity guaranteed the bandwidth of 30 Hz.

RTAI-LAB module compatible with Linux provided the platform to perform the real-time data acquisition in the time domain. Aeroservoelastic state space model built for numerical analysis can be replaced by built-in blocks essential for hardware-software connection. More details about RTAI can be found in [27].

6 BUFFET LOAD MITIGATION SYSTEM

Buffet load mitigation system aims to create active control for actuators to suppress structural vibrations. Thanks to control surfaces on the leading and trailing edges, lift distribution can be altered to attenuate the vibrations in first bending and first torsion modes. In the implementation of static output feedback, the control system has bounded the actuator to move proportionally to the structural velocity. Four different techniques of control systems were tested under BLMS, each of them is explained in the next subsections. All the results presented hereafter will be experimental.

6.1 Buffet Load Mitigation system (BLMS I)

The control law formulation along with optimization strategy defined in the preceding sections constitutes the first part of the research, Buffet Load Mitigation system (BLMS I). Bending and torsional modal accelerations resulted from combination of the signals from accelerometers, were used to suppress modal vibrations [17]. The method followed in the current research is more conservative for control schematic implementation. Maximum weightage was given to accelerometer on the trailing edge at the wing tip as it is farthest from the elastic axis. The structural acceleration for first bending and first torsion modes are given as follows:

$$\begin{Bmatrix} \text{Ben} \\ \text{Tor} \end{Bmatrix} = \begin{bmatrix} 0 & 1 \\ 1 & -1 \end{bmatrix} \begin{Bmatrix} \text{Acc}_{\text{LEI/O}} \\ \text{Acc}_{\text{TEI/O}} \end{Bmatrix} \tag{18}$$

Structural velocities from the respective accelerometers can be derived by integrating with the pseudo integrator of the type (high pass filter):

$$v(s) = \frac{\omega_f^2 s}{s^2 + 2\xi_f \omega_f s + \omega_f^2} a(s) \tag{19}$$

It diminishes the marginal stability introduced by the pure integrators. Initially, the optimization problem on hand was not well posed as the control authority exceeded the physical constraint (saturation) associated with the motor. As stated in [9], without compromise on generality, the weighting functions for external disturbances, feedback outputs and performance index can be set to unity (see equations 11, 12). The control effort can be set arbitrarily to meet the physical constraints of the actuator by iteratively designing the weighing functions to provide the feasibility to wide range of performance based solutions. Figure 8, shows the structural cross spectral power density of four accelerometers attached on the wing, it shows the bending and torsion modes during the experimental tests.

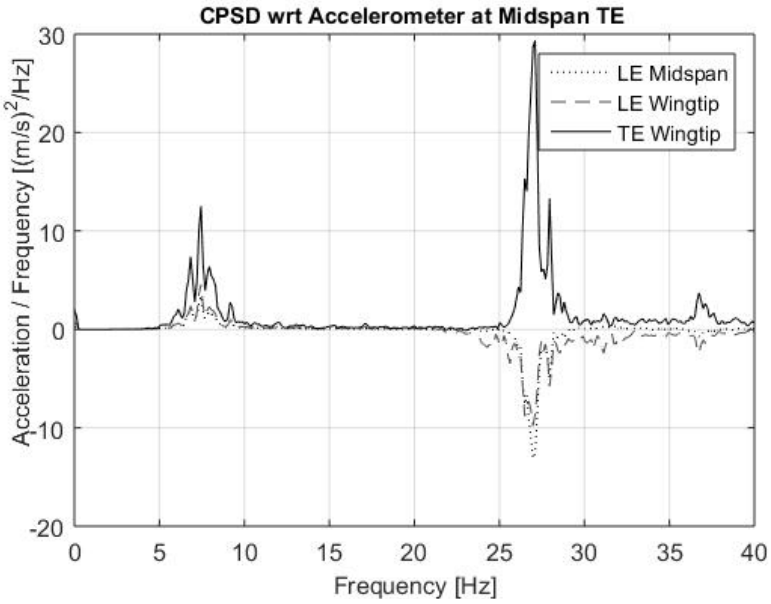

Figure 8: Cross power spectral density of accelerometers

Figure 9, shows the PSD for active control systems with data acquisition from wingtip accelerometer, with all the actuators and sensors working. The dominant peak in the frequency response corresponds to first bending and first torsion modes. The response of the closed loop system is highly damped and significantly attenuated due to the action of the control.

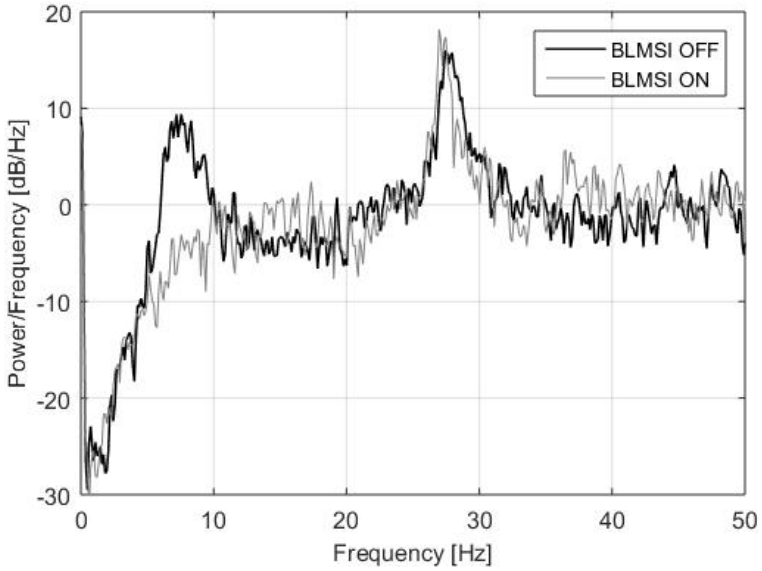

Figure 9: Active control Off/On

Figure 10 shows the efficiency of actuators in case of gains and phase delays. Figures 11(a) and 11(b) are presented here to show that the active control satisfied the mechanical and electrical constraints of the system. For power applied during the active control, the constraints for all the surfaces are well within saturation limit of 10V. As it can be seen in figure 11(b), the LE and TE torques are within the saturation limit of 0.4 Nm and 0.1 Nm respectively.

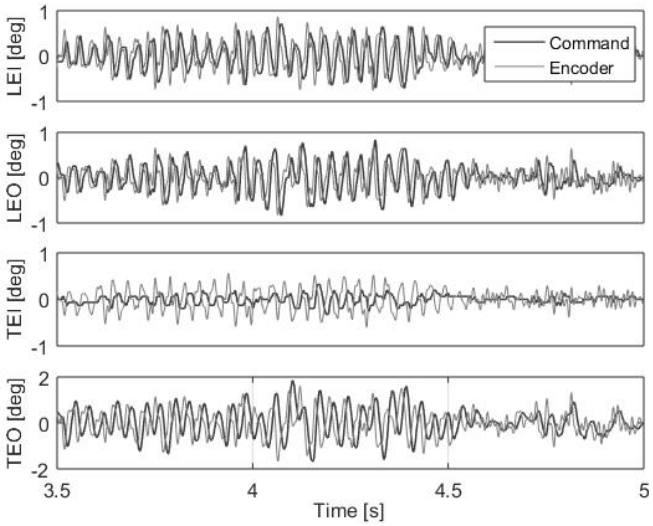

Figure 10: Command and encoder rotations

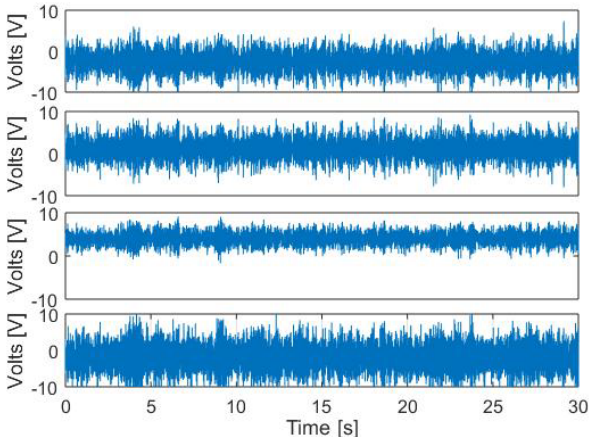

Figure 11(a): Power applied during active control

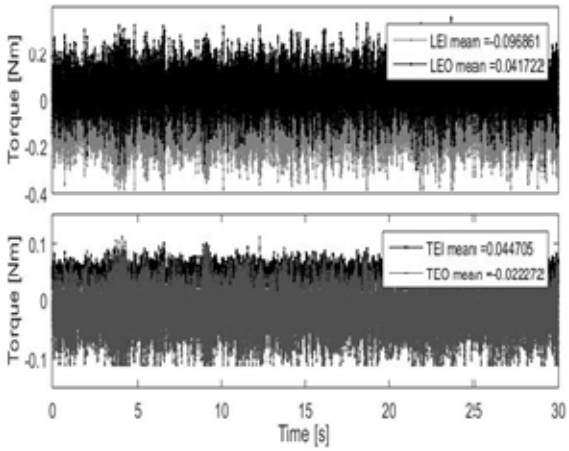

Figure 11(b): Torques of actuators

6.2 Buffet Load Mitigation system II (BLMS II)

A unifying theme to this phase is the usage of Hankel singular values for quantitative attenuation analysis of actuator and sensor combination. Integrated design perspective is presented for this research. Modal analysis is usually carried out by infusing the structure with light or no damping. In [28], it showed that for lightly damped structure, its modal properties can be used to obtain HSV for modal coupling at preliminary design phase, given by the simple expression:

$$\sigma_{yui}^2 = \frac{[b_i^T b_i][c_i^T c_i]}{(4\zeta_i \omega_i)^2} \tag{20}$$

With ‘b’ as the input and ‘c’ as output, denominator defines the time constant of the state as:

$$\tau_i = \frac{1}{(\zeta_i \omega_i)} \tag{21}$$

The numerator provides the coupling of actuator and sensor for the respective mode. So, the task on hand was now to find the suitable combination for modal attenuation, the equation was transformed to find the effective coupling of actuators and sensors to damp out the first bending and first torsion modes.

$$\sigma_{yui}^{\ 2} = \frac{(b_{i_{on}})(c_{i_{on}} / c_{i_{off}})(c_{i_{on}})}{(4\xi\omega_n)^2} \tag{22}$$

For the predetermined actuator sensor locations, the optimum coupling path of actuator signal and sensor output between each mode N_m is given as:

$$\sigma_{yu} = \mathrm{diag}(\sigma_{yu1},...,\sigma_{yun},...,\sigma_{yuNm}) \tag{23}$$

[18], suggested to improve the performance of control, by coupling each mode with performance-disturbance path as:

$$\sigma_{zw} = \mathrm{diag}(\sigma_{zw1},...,\sigma_{zwn},...,\sigma_{zwNm}) \tag{24}$$

In design metric form, it is given as:

$$J_{qp} \equiv \sum_{i=1}^{N_m} \frac{\sigma_{y_p u_q i}^2}{\overline{\sigma}_{yui}^2} \sigma_{zwi}^2 \tag{25}$$

The essence of this task was to select the best couple of q-th sensor and p-th actuator for increase performance and efficiency. $\overline{\sigma}_{yui}^2$ defines the square of all HSV values for actuator/sensor coupling. A similar approach has been adopted to minimize the variance of the outputs: [29] showed that performance ‘z’ can be controlled by introducing the weighting function in the method with systems performance. Design metric can be utilized to switch between the robustness and performance based cost functions. Tables 4-6, are mentioned below to signify the importance of each actuator, table 4 shows the predicted numerical absolute attenuation carried out by each actuator.

Control surface	Bending mode	Torsion mode
LEI	15.83	5.60
LEO	4.799	0.18
TEI	38.04	15.92
TEO	82.01	×

Table 4: Attenuation percentage

Effective performance factor (table 5) can be extracted by normalizing the attenuation with the variance of each actuator during experiment. Significance of actuator/sensor combination for cost function is presented in table 6, it can be readily seen that outboard trailing edge is

more effective in bending mode participating frequencies while inboard trailing edge is more effective in torsional mode attenuation. Moreover, it was also noted the deficiency of leading edge strip i.e. LEO and LEI, as compared to trailing edge strip i.e. TEO and TEI, to cater the turbulent loads produced by the airbrake.

Sensor Location / Control surface	Bending Mode	Torsion Mode
Midspan LEI / LEI	4.711	1.665
Wingtip LEO/ LEO	2.661	0.105
Midspan TEI/TEI	10.91	4.650
Wingtip TEO/ TEO	14.94	×

Table 5: Effective performance factor

Sensor Location / Control surface	Bending Mode	Torsion Mode
Midspan LEI / LEI	×	0.118
Wingtip LEO/ LEO	0.108	0.634
Midspan TEI/TEI	0.360	1.760
Wingtip TEO/ TEO	2.032	×

Table 6: Hankel singular value analysis

Figure 12, shows the variance of velocities before and after the BLMS is switched on for outboard accelerometers and outboard control surfaces.

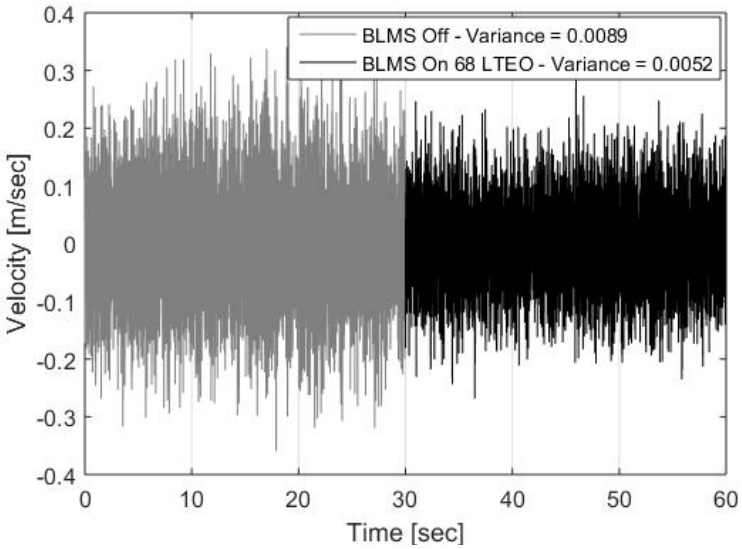

Figure 12: Variance of outboard accelerometers

Table 7, shows the summary of numerical and experimental results. Comparison is drawn in terms of absolute attenuation achieved in frequency response between turbulent force and outboard trailing edge accelerometer.

Control surface	Bending mode	Torsion mode
Numerical	82.01	4.12
Experimental	79.40	1.50

Table 7: Numerical and Experimental comparison

Effectiveness of each control surface is shown in figure 13. It is further highlighted the in-effectivenss the inboard and leading edge strips as comapred to to the outboard and trailing edge strips. (5, 6, 7, 8) in the above figure refers to accelerometers postions located at midspan leading edge, wingtip leading edge, midspan trailing edge and wingtip trailing edge respectively.

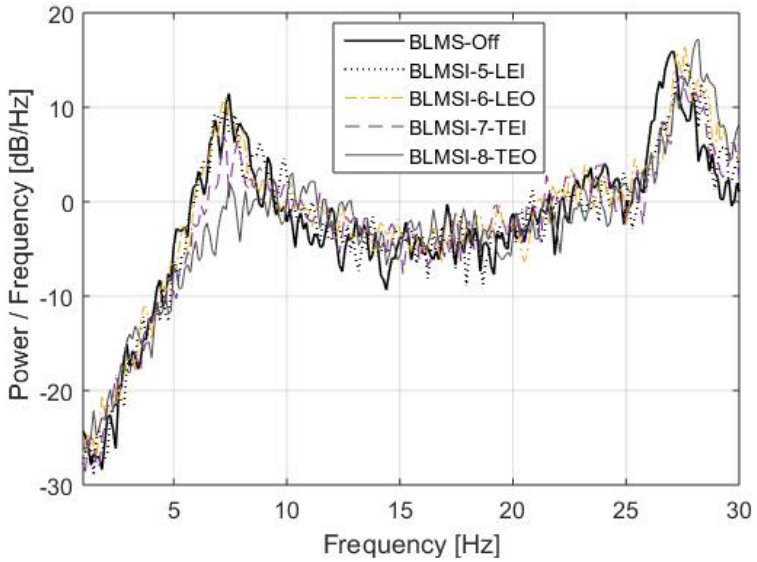

Figure 13: BLMS II for each control surface

6.3 Buffet Load Mitigation system III (BLMS III)

Application of Notch filters is presented in this subsection; it was numerically designed by selecting suitable parameters for notch/peak filter transfer function, experimentally it was validated in Buffet load mitigation system III. The motivation for using a notch and peak filter in the output feedback is to attenuate the participating frequencies in the torsional mode, since it is a source of dynamic instability and needs to be addressed, these filters were incorporated due to the fact of their inclusion does not affect the low frequency and transient behavior of the overall system [11].

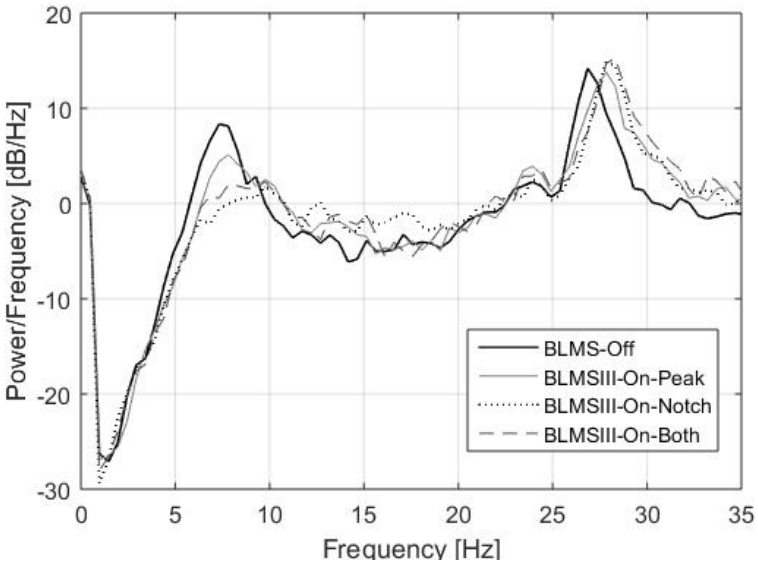

Figure 14: Application of Filters

Preliminary numerical results showed the efficiency of outboard trailing edge in the bending mode but its adverse effect in the torsional mode. Several possibilities exist to achieve the target like dictating the role of trailing edge in the input weighing functions. The proposed method is to form the bending and torsional signals, to be passed out to output feedback of the system, which are processed by peak filter and notch filter at the torsional mode. Improvements were noted for torsional signal with peak filter as shown in figure 14, it indicates the application of notch/peak filters specifically on torsional mode with only active trailing edge outboard actuator.

6.4 Buffet Load Mitigation system IV (BLMS IV)

The performance and robustness of the system is limited by the amount of uncertainty [13]. This robustness of the optimization algorithms ensures the robustness of the optimized control. The resulting controller was tested with respect to forced uncertainties and fixed initiation point for algorithm. The targets for uncertainty were related to instrumentation, accelerometers and actuators, which are more prone to changes over the life span. Numerical uncertainty was introduced in the transfer functions of actuators by changing damping ratio and natural frequency, experimentally it was done by adding on the efficiency factor on the PID_2. While for accelerometers, output feedback was adjusted with the appropriate gains, experimentally it was achieved by changing the sensitivity of the accelerometer and multiplying the accelerometer signal with the varying gain. The numerical results showed promise of the optimization algorithm to handle the uncertainty well. Later it was validated by experimentation conducted under Buffet Load Mitigation system IV.

The test section velocity of the wind tunnel for this campaign was set at 20 m/s, due to safety issues. Figures 15 and 16 shows the power spectral density response of accelerometers for induced uncertainty and the behavior of control to manage the robustness of the system. The optimal solution provided by the algorithm, with same initiation point was still in feasible region. It was noted that outer trailing edge was more prone to uncertainty in the actuator dynamics as compared to other control surfaces. Figure 15, shows the PSD of trailing edge wingtip accelerometer for trailing edge sensitivity (TES). It can be seen in the figure that the performance of the system decreased with the increment in the uncertainty, especially in torsional mode.

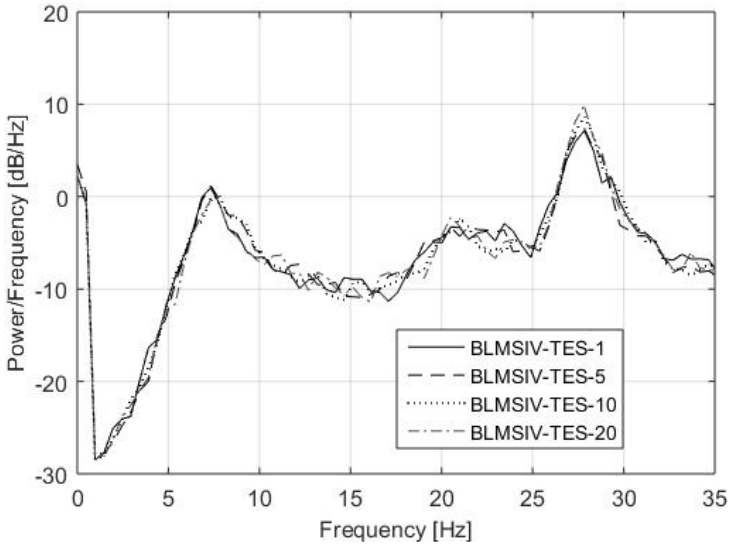

Figure 15: Trailing edge sensitivity for accelerometer certainty

Figure 16, illustrates the performance of active control system with uncertainty in the trailing edge wingtip accelerometer sensitivity. It again shows the decrease in performance of the outer trailing edge to attenuate the loads with the increased uncertainty in the instrumentation.

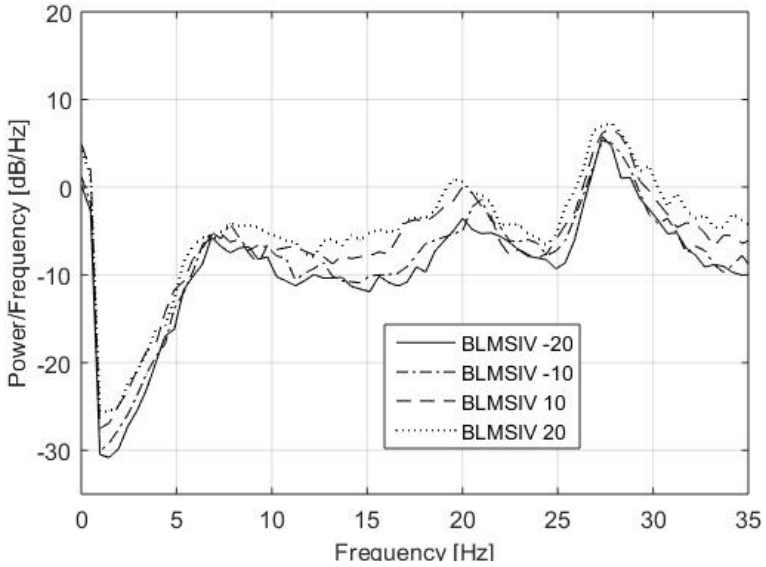

Figure16: Certainty in the accelerometer sensitivity

7 CONCLUSION

This paper presented a control system named as buffet load mitigation system, modelled numerically and validated experimentally. The aim was to attenuate the first bending and the first torsional modes excited by the buffeting loads: for this purpose, an airbrake was built to replicate the buffeting loads on the X-DIA wing. A numerical formulation of a modal control systems based on a static output feedback controller was developed, relying on an optimization provided by heuristic techniques. The aeroservoelastic model was tuned based on previous wind tunnel tests on the X-DIA wing. The formulated numerical model not only showed a promise to attenuate the first bending and torsional modes but it also predicted the effective performance of each control surface and robustness of the system under parametric uncertainties in actuators and sensors. The experimental tests validated the results, which were in good agreement with the predicted numerical simulations.

BLMS I showed the attenuation of approximately 14dB for the first bending mode, while the performance was not satisfactory for the first torsional mode 1dB. BLMS-II compared the performances of the control surfaces, demonstrating that the leading-edge strip control surfaces are less efficient in the attenuation of the wing vibrations under buffeting. Moreover, the performances of inboard control surfaces are relatively less as compared to outboard control surfaces; while the outboard trailing edge is far more effective in controlling the bending mode, the inboard trailing edge performs better in attenuating the torsional mode vibrations. Irrespective of comparison drawn by Hankel singular values, all the surfaces showed attenuation and damped responses for active control system. Improvement of 1dB in the attenuation of the outboard trailing edge was noted in BLMS III. Dedicated tests were conducted to assess the robustness of the system: for the adopted approach the robustness of the system under parametric uncertainty was predicted numerically and later validated experimentally. A decrement of 2.5dB and 2dB was noticed for 20% uncertainty in the actuator transfer function and sensor sensitivity respectively.

Future work will include the upgraded numerical model for PID_2 to cater the overshoot in the response, based on 4th order approximation of Bessel filter. Dedicated Mu-Analysis for robustness is under development and it will be incorporated in the main program. Comparative analysis of control surfaces based on power consumption has enabled the developed system to be coupled to flight mechanics system with optimized power consumption: this task can be accomplished in the future by readily switching different control surfaces for different operational tasks.

8 REFERENCES

[1] Burnham, J. K. Pitt, D. M. White, E. H. Henderson, D. A. and Moses, R. A. (2001). An Advanced Buffet Load Alleviation System 42nd *AIAA structures, structural dynamics and materials conference and exhibit*, Seattle, WA.

[2] John, H. (1974). Critical Review of Methods to Predict the Buffet Penetration Capability of Aircraft, Messerschmitt-Bolkow-Blohm GmbH, Munich, Germany.

[3] Lucia, D. J. (2005). The Sensocraft Configurations: A Non-Linear Aeroservoelastic Challenge for Aviation, Proceedings of the 46th *AIAA/ASME/ASCE/AHS/ASC Structures, Structural Dynamics and Materials Conference,* AIAA, Reston, VA.

[4] Liebeck, R. H. (2004). Design of the Blended Wing Body Subsonic Transport, *Journal of Aircraft,* Vol. 41, No. 1, pp. 10–25.doi:10.2514/1.9084

[5] Eller, D. and Heinze, S. (2004). An Approach to Induced Drag Reduction and its Experimental Evaluation, Proceedings of the 45th *AIAA/ASME/ ASCE/AHS/ASC Structures, Structural Dynamics and Materials Conference*, AIAA, Reston, VA.

[6] Pendleton, E. Bessette, D. Field, P. Miller, G. and Griffin, K. (2000). Active Aeroelastic Wing Flight Research Program: Technical Program and Model Analytical Development, *Journal of Aircraft*, Vol. 37, No. 4, pp. 554–561. doi:10.2514/2.2654

[7] Fonte, F. Ricci, S. and Mantegazza, P. (2015). Gust Load Alleviation for a Regional Aircraft Through a Static Output Feedback, *Journal of Aircraft*, Vol. 52, No. 5, pp. 1559-1574.

[8] Patil, M. J. and Clark, R. L. (2002). Aeroelastic Control Using Multiple Control Surfaces,43rd *AIAA/ASME/ASCE/AHS/ASC Structures, Structural Dynamics, and Materials Conference*, Denver, Colorado.

[9] Dowell, E. H. (2015), *A Modern Course in Aeroelasticity, Solid Mechanics and its Applications*, DOI 10.1007/978-3-319-09453-3_12.

[10] Athalye, A. M. and Grantham, W. J. (1995). Notch Filter Feedback Control of a Chaotic System. *American Control Conference.*

[11] Douglas, B. (2015, 02, 08). Understanding the Sensitivity Function. Retrieved from https://www.youtube.com/watch?v=BAWdZvF1O40

[12] Xing, W. and Singh, S. N. (2000). Adaptive Output Feedback Control of a Nonlinear Aeroelastic Structure, *Journal of Guidance, Control and Dynamics*, Vol. 23, No. 6, pp 1109 – 1116.

[13] Brezina, L. and Brezina, T. (2011). H-Infinity Controller Design for a DC Motor Model with Uncertain Parameters. Engineering Mechanics, Vol. 18, No. 5/6, pp. 271 – 279.

[14] Gu, D.-W. Petkov, P. H. and Konstantinov, M. M. (2005). Robust control Design with MATLAB.

[15] Malecek, J. Cecrdle, J. Scotti, A. Ricci, S. Kiessling, F. and Klimmek, T. (2005). Dynamic Response Analysis and Experimental Validation of the X-DIA Demonstrator Component Model, Proceedings of the IFASD International Forum on Aeroelasticity, *International Forum on Aeroelasticity and Structural Dynamics*, Munich, Germany.

[16] Ricci, S. Scotti, A. Malecek, J. and Cecrdle, J. (2005). Experimental Investigations of a Vibration Suppression System for a Three Surface Aeroelastic Model, Proceedings of the 46th *AIAA/ASME/ASCE/AHS/ ASC Structures, Structural Dynamics and Materials Conference*, AIAA, Reston, VA, 18–21.
[17] De Gaspari, A. Ricci, S. Riccobene, L. and Scotti, A. (2009). Active Aeroelastic Control Over a Multisurface Wing: Modeling and Wind-Tunnel Testing, *AIAA Journal*, Vol. 47, No. 9.
[18] Scotti, A. Ricci, S. Quaranta, G. (2005). Active control of a Three Surface Wind tunnel Aeroelastic Demonstrator: Modelling and Correlations, Proceedings of the IFASD International Forum on Aeroelasticity, *International Forum on Aeroelasticity and Structural Dynamics*, Munich, Germany.
[19] Fonte, F. (2013). *Active gust alleviation for a Regional Aircraft through Static Output Feedback,* Masters Research Thesis.
[20] Roger, K. (1977). Airplane Math Modelling Methods for Active Control Design, *AGARD* CP-228.
[21] Morino, L. Mastroddi, F. De Troia, F. Ghiringhelli, G. L. and Mantegazza, P. (1995). Matrix Fraction Approach for Finite state aerodynamic modelling. *AIAA Journal*, vol. 33, No. 4, pp 703 – 711.
[22] Smith, C. C. and Clark R. L. (1999). Tradeoff in design complexity, temporal vs spatial compensation. J Sound Vib 228(5):1182-1194
[23] Vipperman, J. S. Clark, R. L. Conner M. Dowell EH. (1999). Experimental active Control of Typical Section by using a Trailing Edge Flap. J Airer 35(2):224-229.
[24] Nocedal, J. and Wright, S. J. (2010). *Numerical Optimization,* 2nd Edition, pp 72 – 80.
[25] Gobbi, M. (2015). Course Lectures, Algoritmi Evoluti, *Metodi Di Ottimizzazioni.*
[26] Kelley, C. T. (1999). *Iterative Methods for Optimization, SIAM, Philadelphia, 1999, pp 47,71.*
[27] Dozio, L. and Mantegazza, P. (2003). Real Time Distributed Control Systems Using RTAI, *Proceedings of International Symposium on Object-Oriented Real-Time Distributed Computing*, ISORC, Hakodate, Japan, pp. 11–18.
[28] Williams, T. (1990). Closed form gramian and model reduction for space structures. *IEEE Trans Automatic Control.* 35(3):379 – 382.
[29] Lim, K. B. (1997). Disturbance rejection approach to actuator and sensor placement. *Journal of guidance, control and Dynamics*. 19(6):1370 – 1377.

COPYRIGHT STATEMENT